

## SUPPORT VECTOR MACHINE SKIN LESION CLASSIFICATION IN CLIFFORD ALGEBRA SUBSPACES

MUTLU AKAR, Istanbul, NIKOLAY METODIEV SIRAKOV, Commerce, TX

Received October 23, 2018. Published online October 1, 2019.

*Abstract.* The present study develops the Clifford algebra  $Cl_{5,0}$  within a dermatological task to diagnose skin melanoma using images of skin lesions, which are modeled here by means of 5D lesion feature vectors (LFVs). The LFV is a numerical approximation of the most used clinical rule for melanoma diagnosis - ABCD. To generate the  $Cl_{5,0}$  we develop a new formula that uses the entries of a 5D vector to calculate the entries of a 32D multivector. This vector provides a natural mapping of the original 5D vector onto the 2-, 3-, 4-vector  $Cl_{5,0}$  subspaces. We use a sample set of 112 5D LFVs and apply the new formula to calculate 112 32D multivectors in the  $Cl_{5,0}$ . Next we map the 5D LFVs onto the 2-, 3-, 4-vector subspaces of the  $Cl_{5,0}$ . In every subspace we apply a binary support vector machine to classify the mapped 112 LFVs. With the obtained results we calculate six metrics and evaluate the effectiveness of the diagnosis in every subspace. At the end of the paper we compare the classification results, obtained in every subspace, with the results obtained by the four diagnosing rules most used in clinical practice and contemporary machine learning methods. This way we reveal the potential of using Clifford algebras in the analysis and classification of medical images.

*Keywords:* Clifford algebra; multivector; subspace; classification; skin lesion

*MSC 2010:* 15A66, 08A70, 92B05

### 1. INTRODUCTION

Lately, the rate of melanoma, the deadliest skin cancer, has been expanding [5]. In the US, 1 of every 50 people will develop malignant skin cancer (melanoma) and approximately every 6th one of the cases will be fatal [2], bringing the number of such cases to 9000 per year in the US alone [11]. Luckily, in its early stages,

---

This research was partially supported by the Scientific and Technological Research Council of Turkey (TÜBİTAK) with the scholarship (No. 1059B191800442) through Assistant Prof. Dr. Mutlu Akar.

melanoma is fully curable and making a complete examination of the human body, with a dermoscope or other visual devices, is the most common clinical screening for melanoma diagnosis. Furthermore, the economical effect of melanoma is significant. The minimal treatment cost for stage I is about \$ 2 100 while the minimum cost for stage IV is about \$ 34 000 and could rise to \$ 154 000, see [10]. This is why the problem of early melanoma detection attracts the attention of a number of researchers who delivered a plethora of papers raging from features extraction to skin lesion automated classification [12], [16], [22], [23].

Korotkov [13] proposed an extended categorization of pigmented skin lesion feature descriptors, associating them with automated methods for diagnosing melanoma and classifying clinical and dermoscopic images. Dermoscopy image analysis (DIA) is a developing field. A recent survey investigated the features that have been used in DIA [5]. The study distinguished between skin lesion description features with clinical meaning and features extracted by deep learning techniques.

Image-based computer aided diagnosis systems have huge potential for screening and early recognition of malignant melanoma. The state of the art in these systems and an examination of the current practices, problems, and prospects of image acquisition, preprocessing, segmentation, feature extraction, feature selection, and classification of dermoscopic images have been discussed in [5], [13], [15].

Hermann Günther Grassmann (1809–1877) defined exterior algebra, or Grassmann algebra whose product is the exterior. William Rowan Hamilton (1805–1865) discovered the quaternion algebra to represent the 3-dimensional (3D) rotation. William Kingdon Clifford (1845–1879) merged the above systems to develop the geometric algebra [25]. It is known that Clifford algebra (CA) can be expressed as direct sums of quaternion algebras. Hence, quaternion algebras ( $Cl_{0,2}$ ) can be considered as a special case of the CA. Multivectors are CA structures which map an  $n$ D vector to a  $2^n$ D vector [14], [20]. The CA basis, introduced with (2.3), could be used to define two 1D and  $(n - 1)$  real value subspaces whose dimensions range from  $n$ D to  $\binom{n}{n/2}$ D for  $n$  even and  $\binom{n}{(n-1)/2}$ D for  $n$  odd. The multivector provides a mapping of the original  $n$ D vector onto the CA subspaces.

Given that, extending the dimensionality of a set of vectors leads to an increase of their separability that motivated us to map LFVs to higher dimension subspaces defined by CA multivectors.

Hence, using the 5D LFVs from [23], we define the CA  $Cl_{5,0}$  multivectors developing a new formula to calculate their coefficients (entries). We use them to determine the image of every 5D LFV in the  $Cl_{5,0}$  2-, 3-, 4-vector subspaces. In each subspace a binary support vector machine (SVM) classifies the images as malignant or benign. Hence, the novelties of the present study are:

1. We develop a formula to calculate  $Cl_{5,0}$  multivector coefficients (Section 4).

2. The  $Cl_{5,0}$  multivector defines mappings from  $\mathbb{R}^5$  onto the 2-, 3-, 4-vector CA subspaces with dimensions 10 and 5, respectively. Also, using Clifford product we define a mapping from  $\mathbb{R}^5$  onto 11D CA subspace (Section 3).

To validate the theoretical concepts we use a set of 54 malignant melanoma and 58 benign skin lesion images from [4] diagnosed upon the agreement of three dermatologists. The original images, from which the 5D LFVs are extracted [16], [17], [23], have the size of  $768 \times 512$  pixels and are obtained under the same light conditions.

The remainder of the paper is organized as follows: Section 2.1 is a survey on contemporary classification methods and defines the 5D LFVs; Section 2.2 introduces the basics of the multivectors of the CA  $Cl_{r,s}$ ; Section 3 creates the CA  $Cl_{5,0}$  and its 11D subspace; Section 4 develops a new formula to calculate the  $Cl_{5,0}$  multivector and defines its mappings onto the  $Cl_{5,0}$  2-, 3-, 4-vector subspaces; Section 5 presents experimental results and their statistical evaluation; the last section discusses the contributions, the advantages and the bottlenecks of the present approach, and compares it with recent machine learning methods and rules for clinical diagnosis of melanoma, Appendix calculates the confidence intervals.

## 2. BACKGROUND OF THE STUDY

**2.1. Skin lesion classification.** Papers [13], [15], [16] presented a number of binary classifiers applied to automatically diagnose a skin lesion as benign or malignant: nearest neighbor, decision tree, neural network (NN), Bayesian learning, SVMs, mean shift, and random forest. The review presented in [15] claimed that SVM classifiers are commonly able to outperform NNs.

In [22] Singh and Gupta studied computer-aided diagnosis methods to estimate the melanoma risk in early screening. Also, the paper introduced the state of the art of smartphone-based methods for skin lesion screening.

Wahba et al. [26] developed a novel technique to determinate four pre-defined skin lesion classes. The asymmetry, border irregularity, number of color regions and dots (some dermatologists use lesion diameter) are summed up as the ABCD rule, the most used one in clinical practice to separate melanoma from benign lesions [19]. The method in [26] improved the ABCD rule to also classify basal cell carcinoma and pigmented benign keratoses.

In recent years, the NN methodology gained momentum and a number of papers have been published on the subject [11], [12], [24]. A convolutional NN (CNN) with discriminative regularization is presented in [24]. The CNN classified 170 images with clinical ground truth. It used 75% of them for training and 25% for testing, and received 77.1% accuracy.

Yu et al. [27] presented a novel framework for dermoscopy image recognition via a deep learning method and a local descriptor encoding strategy. The deep representations of rescaled dermoscopy images are first extracted via very deep residual NN, pre-trained on a large natural image dataset. The method in [27] generated a number of discriminative features to deal with the variations within melanoma classes and the variations between melanoma and non-melanoma classes.

In [23] the authors automatically extracted 11 skin lesion features (LFs) and created an 11D LFV that annotates the skin lesion image. They studied the problem of feature selection with respect to the melanoma classification and applied the SVM Recursive Feature Elimination, Information Gain, and Correlation-Based Feature Subset Selection methods on 52 malignant and 50 benign lesion images [23] with a ground truth. As a consequence, the authors determined that the most significant LFs for automatic melanoma classification are:

- $A_B^M$ —the lesion boundary asymmetry about its major axis;
- $A_C^M$ —asymmetry of the union of skin lesion color regions about its major axis;
- $C$ —the number of skin lesion color regions;
- $B$ —the lesion abrupt boundary;
- $D$ —the number of dots and globules present in the lesion.

Hence [23] described a skin lesion image as an 5D LFV:  $(A_B^M, A_C^M, B, C, D)$ , whose entries are similar to those used by the ABCD rule [4], [19]. Analogous findings have been presented in the recent survey [5]. It states that the “hand-crafted features” most important in clinical use are: shape symmetry; color and structure symmetry; boundary features; and color features. Further, [5] determined that dots and globules are important clinical features as well.

Paper [23] applied the binary SVM from [16] and classified 52 malignant and 50 benign 5D LFVs. Paper [23] reported 100% model F-measure, and 88.29% leave one out, and 10-fold cross validation F-measures. In [17] the authors designed a ternary SVM and classified 54 malignant, 38 dysplastic nevi and 20 benign skin LFVs. Considering melanoma as a positive class, dysplastic nevi and benign skin lesions as a negative one, the ternary SVM classified the 112 skin LFVs with the accuracy of 84%.

In the present study we explore CA properties like geometric products and subspaces, where we project the original 5D LFVs. In every subspace we define a binary SVM and automatically classify the mappings of the original 5D LFVs.

**2.2. Clifford algebra subspaces.** This section introduces CA definitions and concepts we apply to develop a new formula for multivector coefficients calculation.

**Definition 2.1.** The *real* CA  $\text{Cl}_{r,s}$  is the algebra generated by the orthonormal basis  $\{e_1, e_2, \dots, e_n\}$  in  $\mathbb{R}^n$  where  $r + s = n$  with (cf. [14], [18], [20], [21]):

$$(2.1) \quad e_i^2 = 1, \quad i = 1, \dots, r, \quad e_i^2 = -1, \quad i = r + 1, \dots, n,$$

$$(2.2) \quad e_i e_j = -e_j e_i, \quad i, j = 1, \dots, n, \quad i \neq j.$$

The CA  $\text{Cl}_{r,s}$ , where  $r + s = n$ , is itself a vector space of dimension  $\sum_{p=0}^n \binom{n}{p} = 2^n$  with the basis

$$(2.3) \quad \{1, e_1, \dots, e_n, e_1 e_2, \dots, e_{n-1} e_n, \dots, e_1 e_2 \dots e_n\}.$$

The elements of the CA  $\text{Cl}_{r,s}$  are named *multivectors* and defined as

$$(2.4) \quad \mathcal{A} = A_{0i} + A_{1i} e_1 + \dots + A_{pi} e_p + A_{2i} e_1 e_2 + \dots + A_{2i} e_{n-1} e_n + \dots + A_{ni} e_1 e_2 \dots e_n,$$

where  $i = \binom{n}{p}$ ,  $p = 0, 1, 2, \dots, n$ , for the coefficients  $A_{pi}$ , which are just notations in (2.4). It follows that the total number of coefficients in (2.4) is  $\binom{n}{0} + \binom{n}{1} + \binom{n}{2} + \dots + \binom{n}{n} = 2^n$ . Consequently, the vector space  $\text{Cl}_{r,s}$  can be decomposed to  $n + 1$  subspaces of dimensions  $\binom{n}{p}$ :

$$(2.5) \quad \text{Cl}_{r,s} = \Lambda^0 \mathbb{R}^n \oplus \Lambda^1 \mathbb{R}^n \oplus \dots \oplus \Lambda^n \mathbb{R}^n.$$

The elements of the subspace  $\Lambda^p \mathbb{R}^n$  are called *p-vectors*,  $p = 0, 1, 2, \dots, n$ . In particular, 0-vectors are real numbers and  $\dim(\Lambda^0 \mathbb{R}^n) = 1$ . The subspace  $\Lambda^1 \mathbb{R}^n$  has the basis  $\{e_1, e_2, \dots, e_n\}$  and  $\dim(\Lambda^1 \mathbb{R}^n) = n$ . Its elements are named 1-vectors and are equal to the original vectors. The subspace  $\Lambda^2 \mathbb{R}^n$  has the basis  $\{e_1 e_2, e_1 e_3, \dots, e_{n-1} e_n\}$ ,  $\dim(\Lambda^2 \mathbb{R}^n) = \binom{n}{2}$  and its elements are 2-vectors (bivectors). Finally,  $\dim(\Lambda^n \mathbb{R}^n) = 1$ , and its basis is the single vector  $\{e_1 e_2 \dots e_n\}$ . The elements of  $\Lambda^n \mathbb{R}^n$  are *n-vectors* (pseudoscalars), see [3], [6], [14].

The decomposition of the vector space  $\text{Cl}_{r,s}$ , as given by (2.5), allows for the multivector  $\mathcal{A}$  to be written in the form

$$(2.6) \quad \mathcal{A} = \langle \mathcal{A} \rangle_0 + \langle \mathcal{A} \rangle_1 + \dots + \langle \mathcal{A} \rangle_n.$$

In (2.6),  $\langle \mathcal{A} \rangle_p$  is the *p-vector* of the multivector  $\mathcal{A}$  and denotes the projection of  $\mathcal{A} \in \text{Cl}_{r,s}$  onto the subspace  $\Lambda^p \mathbb{R}^n$ , see [3], [14], [20].

**Definition 2.2.** The *Clifford product* or *geometric product* of two vectors  $\mathbf{a}$  and  $\mathbf{b}$  is denoted by  $\mathbf{ab}$  and can be expressed as a sum of its symmetric and antisymmetric parts:

$$(2.7) \quad \mathbf{ab} = \mathbf{a} \cdot \mathbf{b} + \mathbf{a} \wedge \mathbf{b},$$

where  $\mathbf{a} \cdot \mathbf{b}$  is the *inner product* while  $\mathbf{a} \wedge \mathbf{b}$  is the *outer* or *wedge product*.

### 3. THE CLIFFORD ALGEBRA $Cl_{5,0}$

Recall the authors in [16] and [23] developed the 5D LFV  $(A_B^M, A_C^M, B, C, D)$  to describe a skin lesion in an image. Thus, we construct the CA  $Cl_{5,0}$  of  $\mathbb{R}^5$  with an orthonormal basis  $\{e_1, e_2, e_3, e_4, e_5\}$  which satisfies the relations

$$(3.1) \quad e_1^2 = e_2^2 = e_3^2 = e_4^2 = e_5^2 = 1 \quad \text{and} \quad e_i e_j = -e_j e_i \quad \text{for } i \neq j.$$

It follows from Section 2.2, that the  $Cl_{5,0}$  is a  $2^5$ -dimensional algebra with the basis [6]

$$(3.2) \quad \begin{array}{ll} \text{scalar} & 1, \\ \text{1-vectors} & e_1, e_2, e_3, e_4, e_5, \\ \text{bivectors} & e_{12}, e_{13}, e_{14}, e_{15}, e_{23}, e_{24}, e_{25}, e_{34}, e_{35}, e_{45}, \\ \text{3-vectors} & e_{123}, e_{124}, e_{125}, e_{134}, e_{135}, e_{145}, e_{234}, e_{235}, e_{245}, e_{345}, \\ \text{4-vectors} & e_{1234}, e_{1235}, e_{1245}, e_{1345}, e_{2345}, \\ \text{pseudoscalar} & e_{12345}. \end{array}$$

In (3.2) we use the notation  $e_{ij} = e_i e_j$ ,  $e_{ijk} = e_i e_j e_k$ ,  $e_{ijkl} = e_i e_j e_k e_l$ ,  $e_{12345} = e_1 e_2 e_3 e_4 e_5$  [14].

Assume that a skin lesion, in an image, is annotated with the 5D LFV  $U = (u_1, u_2, u_3, u_4, u_5) \in \mathbb{R}^5$  in the basis  $\{e_1, e_2, e_3, e_4, e_5\}$ . According to (3.2),

$$\begin{aligned} Cl_{5,0} = \text{span}\{ & 1, e_1, e_2, e_3, e_4, e_5, e_{12}, e_{13}, e_{14}, e_{15}, e_{23}, e_{24}, e_{25}, e_{34}, e_{35}, e_{45}, e_{123}, \\ & e_{124}, e_{125}, e_{134}, e_{135}, e_{145}, e_{234}, e_{235}, e_{245}, e_{345}, e_{1234}, e_{1235}, e_{1245}, e_{1345}, \\ & e_{2345}, e_{12345}\}. \end{aligned}$$

Using the basis in (3.2) and applying the multivector definition, equation (2.4), we receive the  $Cl_{5,0}$  multivector

$$(3.3) \quad \begin{aligned} A_U = & A_0 + A_1 e_1 + A_2 e_2 + A_3 e_3 + A_4 e_4 + A_5 e_5 + A_6 e_{12} + A_7 e_{13} \\ & + A_8 e_{14} + A_9 e_{15} + A_{10} e_{23} + A_{11} e_{24} + A_{12} e_{25} + A_{13} e_{34} + A_{14} e_{35} \\ & + A_{15} e_{45} + A_{16} e_{123} + A_{17} e_{124} + A_{18} e_{125} + A_{19} e_{134} + A_{20} e_{135} \\ & + A_{21} e_{145} + A_{22} e_{234} + A_{23} e_{235} + A_{24} e_{245} + A_{25} e_{345} + A_{26} e_{1234} \\ & + A_{27} e_{1235} + A_{28} e_{1245} + A_{29} e_{1345} + A_{30} e_{2345} + A_{31} e_{12345} \in Cl_{5,0}. \end{aligned}$$

In (3.3), for the purpose of simplicity, we switch to a consecutive indexing of the coefficients, while in (2.4) we use a subspace related indexing. Applying the Clifford

product and (2.7) and (3.1), we calculate the norm of  $A_U \in \text{Cl}_{5,0}$  [14]:

$$(3.4) \quad |A_U|^2 = |A_0|^2 + |A_1|^2 + |A_2|^2 + |A_3|^2 + |A_4|^2 + |A_5|^2 + |A_6|^2 + |A_7|^2 \\ + |A_8|^2 + |A_9|^2 + |A_{10}|^2 + |A_{11}|^2 + |A_{12}|^2 + |A_{13}|^2 + |A_{14}|^2 \\ + |A_{15}|^2 + |A_{16}|^2 + |A_{17}|^2 + |A_{18}|^2 + |A_{19}|^2 + |A_{20}|^2 + |A_{21}|^2 \\ + |A_{22}|^2 + |A_{23}|^2 + |A_{24}|^2 + |A_{25}|^2 + |A_{26}|^2 + |A_{27}|^2 + |A_{28}|^2 \\ + |A_{29}|^2 + |A_{30}|^2 + |A_{31}|^2.$$

According to (2.5), (2.6), (3.2) and (3.3),  $A_0 \in \Lambda^0\mathbb{R}^5$ , the vector  $(A_1, \dots, A_5) \in \Lambda^1\mathbb{R}^5$  is the 1-vector subspace of the original vectors, the vector  $(A_6, \dots, A_{15}) \in \Lambda^2\mathbb{R}^5$  is the image of  $A_U$  onto the subspace of the bivectors, the vector  $(A_{16}, \dots, A_{25}) \in \Lambda^3\mathbb{R}^5$  is the projection of  $A_U$  onto the  $\text{Cl}_{5,0}$  subspace defined by the 3-vectors, while  $(A_{26}, \dots, A_{30}) \in \Lambda^4\mathbb{R}^5$  is the projection of  $A_U$  onto the 4-vector subspace, and  $A_{31} \in \Lambda^5\mathbb{R}^5$ . It follows that, in order to find the projections of a 5D LFV onto the CA subspaces we have to develop a formula to calculate the multivector coefficients  $A_0, \dots, A_{31}$ .

Assume  $w = (w_1, w_2, w_3, w_4, w_5) = w_1e_1 + w_2e_2 + w_3e_3 + w_4e_4 + w_5e_5 \in \mathbb{R}^5$ , and  $U = (u_1, u_2, u_3, u_4, u_5) = u_1e_1 + u_2e_2 + u_3e_3 + u_4e_4 + u_5e_5 \in \mathbb{R}^5$ . Applying (2.7), we calculate the Clifford product  $wU$  considering that it is non-commutative, but is associative and distributive over addition:

$$wU = (w_1e_1 + w_2e_2 + w_3e_3 + w_4e_4 + w_5e_5)(u_1e_1 + u_2e_2 + u_3e_3 + u_4e_4 + u_5e_5) \\ = (w_1u_1)e_1e_1 + (w_1u_2)e_1e_2 + (w_1u_3)e_1e_3 + (w_1u_4)e_1e_4 + (w_1u_5)e_1e_5 \\ + (w_2u_1)e_2e_1 + (w_2u_2)e_2e_2 + (w_2u_3)e_2e_3 + (w_2u_4)e_2e_4 + (w_2u_5)e_2e_5 \\ + (w_3u_1)e_3e_1 + (w_3u_2)e_3e_2 + (w_3u_3)e_3e_3 + (w_3u_4)e_3e_4 + (w_3u_5)e_3e_5 \\ + (w_4u_1)e_4e_1 + (w_4u_2)e_4e_2 + (w_4u_3)e_4e_3 + (w_4u_4)e_4e_4 + (w_4u_5)e_4e_5 \\ + (w_5u_1)e_5e_1 + (w_5u_2)e_5e_2 + (w_5u_3)e_5e_3 + (w_5u_4)e_5e_4 + (w_5u_5)e_5e_5.$$

Applying (3.1) and (3.2) to the above expression, we arrived at

$$(3.5) \quad wU = (w_1u_1 + w_2u_2 + w_3u_3 + w_4u_4 + w_5u_5)1 \\ + (w_1u_2 - w_2u_1)e_{12} + (w_1u_3 - w_3u_1)e_{13} \\ + (w_1u_4 - w_4u_1)e_{14} + (w_1u_5 - w_5u_1)e_{15} \\ + (w_2u_3 - w_3u_2)e_{23} + (w_2u_4 - w_4u_2)e_{24} \\ + (w_2u_5 - w_5u_2)e_{25} + (w_3u_4 - w_4u_3)e_{34} \\ + (w_3u_5 - w_5u_3)e_{35} + (w_4u_5 - w_5u_4)e_{45} \in \text{Cl}_{5,0}.$$

Consider  $U$  in (3.5) as a 5D LFV and select  $w = [1.3, 1.3, 0.5, 0.1, 0.5]$  to be a vector of weights, which is the same for every LFV from the sample space. Thus, (3.5) maps

every 5D skin LFV to an 11D vector. Note, that the values in  $w$  are the same as the weights adopted by the ABCD rule, the most commonly used rule for melanoma diagnosis in clinical practice [4], [19], [26].

#### 4. CALCULATIONS OF THE $Cl_{5,0}$ MULTIVECTORS

In the present section we propose a new approach to calculating the coefficients of the multivector  $A_U$  defined in the  $Cl_{5,0}$  by (3.3). We consider the vector  $U = (u_1, u_2, u_3, u_4, u_5) \in \mathbb{R}^5$  in the basis  $\{e_1, e_2, e_3, e_4, e_5\}$  and construct the table below by filling up the 1st column with  $u_i e_i, i = \{1, \dots, 4\}$ , and the upper row with  $u_j e_j, j = \{2, \dots, 5\}$ , as shown below. To fill up the lower right part of the table we calculate the Clifford products  $u_i e_i u_j e_j$  for  $i < j$ .

	$u_2 e_2$	$u_3 e_3$	$u_4 e_4$	$u_5 e_5$
$u_1 e_1$	$u_1 u_2 e_{12}$	$u_1 u_3 e_{13}$	$u_1 u_4 e_{14}$	$u_1 u_5 e_{15}$
$u_2 e_2$		$u_2 u_3 e_{23}$	$u_2 u_4 e_{24}$	$u_2 u_5 e_{25}$
$u_3 e_3$			$u_3 u_4 e_{34}$	$u_3 u_5 e_{35}$
$u_4 e_4$				$u_4 u_5 e_{45}$

Further, we construct a second table, where the 1st column contains  $u_k e_k, k \in \{1, 2, 3\}$ , while the upper row consists of the terms  $u_i u_j e_{ij}$ , where the pair  $ij \in \{23, 24, 25, 34, 35, 45\}$ . Next, we fill up the lower right part of the 2nd table conducting right multiplication, such that  $k < i < j$ , in the subscript triplets  $kij$ .

	$u_2 u_3 e_{23}$	$u_2 u_4 e_{24}$	$u_2 u_5 e_{25}$	$u_3 u_4 e_{34}$	$u_3 u_5 e_{35}$	$u_4 u_5 e_{45}$
$u_1 e_1$	$u_1 u_2 u_3 e_{123}$	$u_1 u_2 u_4 e_{124}$	$u_1 u_2 u_5 e_{125}$	$u_1 u_3 u_4 e_{134}$	$u_1 u_3 u_5 e_{135}$	$u_1 u_4 u_5 e_{145}$
$u_2 e_2$				$u_2 u_3 u_4 e_{234}$	$u_2 u_3 u_5 e_{235}$	$u_2 u_4 u_5 e_{245}$
$u_3 e_3$						$u_3 u_4 u_5 e_{345}$

Following the above concepts and rules we construct two new tables as shown below.

	$u_2 u_3 u_4 e_{234}$	$u_2 u_3 u_5 e_{235}$	$u_2 u_4 u_5 e_{245}$	$u_3 u_4 u_5 e_{345}$
$u_1 e_1$	$u_1 u_2 u_3 u_4 e_{1234}$	$u_1 u_2 u_3 u_5 e_{1235}$	$u_1 u_2 u_4 u_5 e_{1245}$	$u_1 u_3 u_4 u_5 e_{1345}$
$u_2 e_2$				$u_2 u_3 u_4 u_5 e_{2345}$

	$u_2 u_3 u_4 u_5 e_{2345}$
$u_1 e_1$	$u_1 u_2 u_3 u_4 u_5 e_{12345}$

Now, we add together the 26 terms from the lower right parts of the above four tables along with the sum  $1 + u_1 e_1 + u_2 e_2 + u_3 e_3 + u_4 e_4 + u_5 e_5$ . Hence, we arrive at



the following expression for the multivector  $A_U$ :

$$(4.1) \quad A_U = 1 + u_1e_1 + u_2e_2 + u_3e_3 + u_4e_4 + u_5e_5 + u_{12}e_{12} + u_{13}e_{13} \\ + u_{14}e_{14} + u_{15}e_{15} + u_{23}e_{23} + u_{24}e_{24} + u_{25}e_{25} + u_{34}e_{34} + u_{35}e_{35} \\ + u_{45}e_{45} + u_{123}e_{123} + u_{124}e_{124} + u_{125}e_{125} + u_{134}e_{134} + u_{135}e_{135} \\ + u_{145}e_{145} + u_{234}e_{234} + u_{235}e_{235} + u_{245}e_{245} + u_{345}e_{345} + u_{1234}e_{1234} \\ + u_{1235}e_{1235} + u_{1245}e_{1245} + u_{1345}e_{1345} + u_{2345}e_{2345} + u_{12345}e_{12345}.$$

Now, we compare the coefficients of the basis vectors in (3.3) and (4.1) and receive:

$$(4.2) \quad A_0 = 1, \quad A_1 = u_1, \quad A_2 = u_2, \quad A_3 = u_3, \quad A_4 = u_4, \quad A_5 = u_5, \quad A_6 = u_1u_2, \\ A_7 = u_1u_3, \quad A_8 = u_1u_4, \quad A_9 = u_1u_5, \quad A_{10} = u_2u_3, \quad A_{11} = u_2u_4, \\ A_{12} = u_2u_5, \quad A_{13} = u_3u_4, \quad A_{14} = u_3u_5, \quad A_{15} = u_4u_5, \\ A_{16} = u_1u_2u_3, \quad A_{17} = u_1u_2u_4, \quad A_{18} = u_1u_2u_5, \quad A_{19} = u_1u_3u_4, \\ A_{20} = u_1u_3u_5, \quad A_{21} = u_1u_4u_5, \quad A_{22} = u_2u_3u_4, \quad A_{23} = u_2u_3u_5, \\ A_{24} = u_2u_4u_5, \quad A_{25} = u_3u_4u_5, \quad A_{26} = u_1u_2u_3u_4, \\ A_{27} = u_1u_2u_3u_5, \quad A_{28} = u_1u_2u_4u_5, \quad A_{29} = u_1u_3u_4u_5, \\ A_{30} = u_2u_3u_4u_5, \quad A_{31} = u_1u_2u_3u_4u_5.$$

Equation (4.2) is a new formula to calculate the coefficients of the multivector  $A_U \in \text{Cl}_{5,0}$  that corresponds to an original vector  $U \in \mathbb{R}^5$ . According to (2.5) and (2.6)  $A_0$  is a scalar, while  $A_{31}$  is a pseudoscalar coefficient. Note that the vectors  $U = (u_1, u_2, u_3, u_4, u_5) = (A_1, \dots, A_5)_U = \langle A_U \rangle_1 \in \Lambda^1\mathbb{R}^5$ ,  $(A_6, \dots, A_{15})_U = \langle A_U \rangle_2 \in \Lambda^2\mathbb{R}^5$ ,  $(A_{16}, \dots, A_{25})_U = \langle A_U \rangle_3 \in \Lambda^3\mathbb{R}^5$ , while  $(A_{26}, \dots, A_{30})_U = \langle A_U \rangle_4 \in \Lambda^4\mathbb{R}^5$ . Equations (2.6), (3.3) and (4.2) imply that  $\langle A_U \rangle_1 = U$ , while  $\langle A_U \rangle_2, \langle A_U \rangle_3, \langle A_U \rangle_4$  are projections of  $U$  onto the 2-, 3-, 4-vector subspaces of the  $\text{Cl}_{5,0}$ .

## 5. EXPERIMENTAL RESULTS

To measure the effectiveness of classification in the CA  $\text{Cl}_{5,0}$  subspaces we use a dataset of 5D LFVs  $(A_B^M, A_C^M, B, C, D) = U_i$  ( $i = 1, \dots, 112$ ) from [17]. The LFVs are extracted from the 54 malignant melanoma and 58 benign skin lesion images from [4], diagnosed upon the agreement of three dermatologists. All images are obtained under same light conditions and have the size of  $768 \times 512$  pixels.

The present study calculates a 32D multivector  $A_{U_i}$  for every 5D LFV  $U_i$  applying (4.2) and projects  $A_{U_i}$  onto the  $\text{Cl}_{5,0}$  2-, 3-, 4-vector subspaces. The calculations are coded in MATLAB.

In Fig. 1 we show two examples of skin lesion images from our collection of 112. The masks of the color regions extracted from the left image are presented as well.

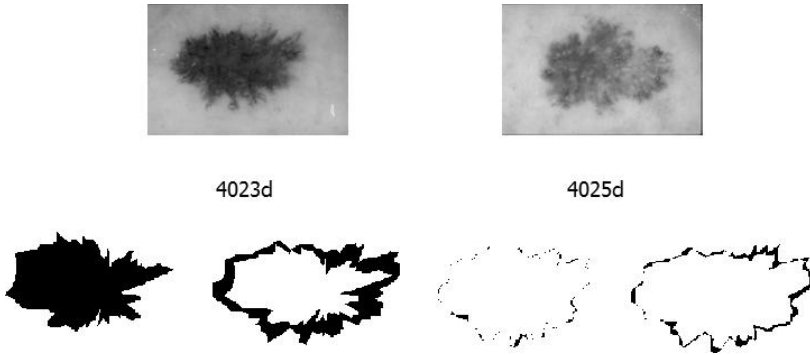


Figure 1. First row: skin lesion images. Second row from left to right: masks of the dark-brown, red, blue-gray, and light-brown color regions extracted from the skin lesion 4023d.

**Example 5.1.** The LFV  $U_1 = (0.848, 0.811, 4, 4, 0.5) \in \mathbb{R}^5$  is calculated using the methods of [16], [17], [23] from the lesion image 4023d shown in Fig. 1. Applying (4.2) we calculate the  $Cl_{5,0}$  multivector

$$\begin{aligned}
 A_{U_1} = \{ & 1, \quad \text{scalar,} \\
 & 0.848, 0.811, 4, 4, 0.5, \quad \text{original vector, 1-vector,} \\
 & 0.688, 3.393, 3.393, 0.424, 3.244, 3.244, 0.405, 16, 2, 2, \quad \text{bivector,} \\
 & 2.752, 2.752, 0.344, 13.574, 1.696, 1.696, 12.976, 1.622, 1.622, 8, \quad \text{3-vector,} \\
 & 11.009, 1.376, 1.376, 6.787, 6.488, \quad \text{4-vector,} \\
 & 5.504, \quad \text{pseudoscalar} \} \in Cl_{5,0}.
 \end{aligned}$$

As we did in Example 5.1, for every LFV  $U_i$  ( $i = 1, \dots, 112$ ) we calculate a multivector  $A_{U_i} \in Cl_{5,0}$ . According to Section 4, the projection of  $A_{U_i}$  onto the: 1-vector subspace  $\Lambda^1 \mathbb{R}^5$  is  $U_i$  (Note: Classification in this subspace is the same as classification of the original LFVs.); bivector subspace  $\Lambda^2 \mathbb{R}^5$  is  $(A_6, \dots, A_{15})_{U_i}$ ; 3-vector subspace  $\Lambda^3 \mathbb{R}^5$  is  $(A_{16}, \dots, A_{25})_{U_i}$ ; 4-vector subspace  $\Lambda^4 \mathbb{R}^5$  is  $(A_{26}, \dots, A_{30})_{U_i}$  for  $i = 1, \dots, 112$ . Hence, we map the original sample set of LFVs onto the above  $Cl_{5,0}$  subspaces. In every subspace we apply  $\nu$ -SVM. The parameter  $\nu \in [0, 1]$  favors the positive samples (malignant) if  $\nu > 0.5$  (produces higher sensitivity) while it favors the negative (benign) samples otherwise (produces higher specificity). Also, we apply the  $\nu$ -SVM with three different kernels (Gaussian, RBF, degree 2 polynomial) and report the results in Tables 1 and 2. The six metrics accuracy (AC), sensitivity

(SE), specificity (SP), precision (PR), recall (RE), and F-measure (F) are calculated for every kernel using 1000 classification experiments.

Kernel	Hold Out %	5D 4-vector		10D bivector		10D 3-vector	
		AC/SE=RE/SP/PR/F	AC/SE=RE/SP/PR/F	AC/SE=RE/SP/PR/F	AC/SE=RE/SP/PR/F		
Gaussian	10	70.7/71.3/69.9/77.6/74.3	79.1/77.6/81.4/86.7/81.9	75.9/76.0/75.9/81.8/78.8			
RBF	10	70.3/70.9/69.5/77.4/74.0	78.2/76.9/80.3/85.9/81.1	76.2/76.4/76.0/81.6/78.9			
Polynomial, $d = 2$	10	68.4/69.9/66.4/74.0/71.9	77.9/77.2/79.0/84.5/80.7	76.2/76.8/75.5/80.9/78.8			

Table 1. Classification results in percent in 2-, 3-, 4-vector  $Cl_{5,0}$  subspaces.

Kernel	Hold Out %	5D 1-vector		11D, [1.3 1.3 0.5 0.1 0.5]	
		AC/SE=RE/SP/PR/F	AC/SE=RE/SP/PR/F	AC/SE=RE/SP/PR/F	AC/SE=RE/SP/PR/F
Gaussian	10	82.4/ 81.3/84.0/ 88.0/ 84.5		78.8/78.6/79.1/84.0/81.2	
RBF	10	83.0/81.6/84.9/88.8/85.1		78.4/78.1/78.8/83.9/80.9	
Polynomial, $d = 2$	10	82.3/81.8/82.8/86.7/84.2		77.7/78.3/76.7/81.6/79.9	

Table 2. Classification results in percent in 1-vector (original 5D LfVs) and 11D subspaces.

The experiment is called a SVM classification using  $x\%$  of samples to train the SVM and  $(100 - x)\%$  of samples to classify with the trained SVM. Note that the repeatability of the SVM classification is not constant if a number of experiments are performed with one and the same dataset and set of parameters. Therefore, the average of all experiments is a reasonable measure to determine the TP (true positive), TN (true negative), FP (false positive), and FN (false negative). The number of experiments under the above settings is called a trail. In the present study we use: trails with 1000 experiments, because the variability of the results is in the order of 0.1% between every two trails;  $\nu = 0.4$ , because the dermatologists are interested in less FP:

$$SE = \frac{TP}{TP + FN}, \quad SP = \frac{TN}{TN + FP}, \quad AC = \frac{TP + TN}{TP + FP + FN + TN},$$

$$PR = \frac{TP}{TP + FP}, \quad RE = \frac{TP}{TP + FN}, \quad F = 2 \times \frac{PR \times RE}{PR + RE}.$$

In the first set of trails we use 90% (101) of the LfVs to train the  $\nu$ -SVM and 10% (11) LfVs to test the trained SVM. We report the results in Tables 1 and 2 in percent. One may tell from this, that the highest values for all the six metrics are obtained by the classification of the original 5D LfVs (1-vectors), while the 2nd highest values are from the classification in the 2-vector subspace. This is due to the fact that the 3rd and 4th entries in the original 5D LfVs are in the range of

[0, 6] and [0, 8], respectively (see Example 5.1) [16], [17], [23]. On the other hand, the 1st, 2nd and 5th entries attain the values in [0, 1]. Thus, the contribution of each entry is different for the classification outcome. Moreover, the new (4.2), developed to calculate the  $Cl_{5,0}$  multivector coefficients, implies that this difference further increases in the bivector, 3-vector and 4-vector subspaces. For example, the 14th entry  $A_{13}$  in (4.2) (the 8th one in the bivector from Example 5.1) is formed by  $u_3u_4$ . Therefore  $A_{13} \in [0, 48]$ . It follows that the multivector projection onto the 2-, 3-, 4-vector subspaces significantly increases the distances among vectors on some coordinate axes, while the distances become very small on other axes. Therefore, the SVM does not accurately split melanoma from benign vectors. As a consequence the classification rates drop in CA  $Cl_{5,0}$  subspaces, as witnessed in Tables 1 and 2.

To remedy the problem we normalize the 3rd (dividing by 6) and 4th (dividing by 8) entry of the original 5D vectors (Example 5.1). Hence we map the values from the 3rd and 4th entries onto [0, 1] (Example 5.2).

**Example 5.2.** The normalized version of the LFV  $U_1$  is  $U_{N_1} = (0.8484, 0.8111, 0.6667, 0.5, 0.5) \in \mathbb{R}^5$ . The  $Cl_{5,0}$  multivector calculated from  $U_{N_1}$  by applying (4.2) is

$$\begin{aligned}
 A_{U_{N_1}} = \{ & 1, \quad \text{scalar,} \\
 & 0.848, 0.811, 0.667, 0.5, 0.5, \quad \text{original vector, 1-vector,} \\
 & 0.688, 0.565, 0.424, 0.424, 0.540, 0.405, 0.405, 0.333, 0.333, 0.25, \quad \text{bivector,} \\
 & 0.458, 0.344, 0.344, 0.282, 0.282, 0.212, 0.270, 0.270, 0.202, 0.166, \quad \text{3-vector,} \\
 & 0.229, 0.229, 0.172, 0.141, 0.135, \quad \text{4-vector,} \\
 & 0.114, \quad \text{pseudoscalar} \} \in Cl_{5,0}.
 \end{aligned}$$

We conduct a trail of experiments applying every kernel on the normalized LFVs  $U_{N_i}$ ,  $i = 1, \dots, 112$ , and their projections onto the 2-, 3-, 4-vector  $Cl_{5,0}$  subspaces. We select 2% (2) of the vectors to test and 98% (110) of the vectors to train the  $\nu$ -SVM and report the results in percent in Tables 3 and 4. One may say that the values increased there according to Tables 1 and 2. Hence the highest accuracy of 84.7%, specificity of 87.2% and sensitivity of 82.4% in Table 4 are higher than the maximal values in Table 2: 83% accuracy, 84.9% specificity and 81.8% sensitivity.

Kernel	Hold Out %	5D 4-vector	10D Bivector	10D 3-vector
		AC/SE=RE/SP/PR/F	AC/SE=RE/SP/PR/F	AC/SE=RE/SP/PR/F
Gaussian	2	72.7 / 67.7 / 77.2/82/79.5	80.3/ 75.8/ 84.3/ 86.5/ 80.8	77.8/ 74/ 80.8/ 83/ 78
RBF	2	71.8 / 67.2/ 75.4/80/77.6	81.9/ 76.1/ 85.3/ 87.5/ 81.4	77/ 72.5/ 81.4/ 72.5/78
Polynomial, $d = 2$	2	71.2/ 66.3 / 75.6/81/73	81.1 / 79.3/ 82.2/83.1/ 81.1	79 / 76.6/ 81/ 82.7/ 79.5

Table 3. Classification results with the normalized sample set in the 2-, 3-, 4-vector  $Cl_{5,0}$  subspaces.

Kernel	Hold	5D 1-vector	11D, [1.3, 1.3, 0.5, 0.1, 0.5]
	Out %	AC/SE=RE/SP/PR/F	AC/SE=RE/SP/PR/F
Gaussian	2	81.8 / 79.1 / 84.1/85.4/ 82.1	81.8/ 75/ 85 / 88/ 81.1
RBF	2	82.5 / 79.8 / 84.5/85.7/ 82.6	81.5/ 77/ 85.9/ 88/ 82
Polynomial, $d = 2$	2	84.7/ 82.4/ 86.4/87.2/ 84.7	84 / 79 / 87.2/ 88.8/ 83.6

Table 4. Classification results with the normalized sample set in 1-vector (normalizes original 5D LFVs) and 11D  $Cl_{5,0}$  subspace.

Note that the highest precision of 88.8% in Table 4 is obtained in the 11D  $Cl_{5,0}$  subspace. The next largest precision of 87.5% (Table 3) comes in the bivector subspace and it is larger than the maximal precision of 87.2% reached with the original 5D LFVs in the 1-vector subspace. Also, the specificity of 87.2% in the 11D subspace is higher than the largest specificity of 86.4% obtained with the original 5D LFVs. These results validate the higher potential of classification in CA subspaces as compared to classification in real valued vector spaces.

Applying (7.1)–(7.3) (see Appendix) we calculate the CIs for the maximal accuracy, sensitivity and specificity from Tables 3 and 4, and report the results in Table 5. Note that the reported CIs are narrow, which is an important statistical feature. We do not show the CI for the non-normalized data, because its classification results are weaker than the results with the normalized sample set.

Subspace	Max	CI
1-vector	AC=84.7	$\widehat{AC} \in [83, 86.4]$
1-vector	SE=82.4	$\widehat{SE} \in [80, 84.7]$
11D	SP=87.2	$\widehat{SP} \in [85, 89.4]$

Table 5. In Appendix we calculate the CI for the AC, SE and SP of the entire population using the maximal values from Tables 3 and 4.

## 6. CONCLUSION

Theoretical contributions of the present study include developing (4.2) to calculate the  $Cl_{5,0}$  multivector coefficients, which define a mapping from  $\mathbb{R}^5$  onto the 2-, 3-, 4-vector CA 10D and 5D subspaces, respectively. Also, using Clifford product we develop (3.5) to map any vector from  $\mathbb{R}^5$  onto 11D CA subspace. In this subspace the classification of 112 skin LFVs demonstrates superior precision 88.8% (Table 4) as compared to the classification of the original 5D LFVs in the 1-vector subspace (Tables 2, 4), and superior specificity as compared to the four diagnosing rules most used by dermatologists (Table 6).

Recall, to validate the theoretical concepts and derive the above conclusions we conducted experiments with 112 5D LFVs extracted from 112 images with ground truth provided by three dermatologists [4]. Applying the new (4.2) we calculated 112 32D lesion feature multivectors and mapped them onto the 2-, 3-, 4-vector CA subspaces where we conducted SVM binary classification.

As we noted in the introduction NNs gained popularity in the classification community and found significant application in skin lesion image classification to benign and malignant [11], [24]. A main drawback of the NNs is the need of large amount of training data to receive high statistical metrics and narrow CIs. For example, in [9] the authors applied the GoogLeNet Inception V3 CNN on about 129 450 skin lesion images to train the NN and on 1942 biopsy labeled images to test the NN. They validated the effectiveness of the algorithm through the classification of the three classes: benign, malignant and non-neoplastic [9]. Hence, the NN provided an overall accuracy of 72.1%, a way lower than the accuracy of 84% in the  $Cl_{5,0}$  11D subspace. Also, the CNN accuracy is lower than the 81.9% accuracy obtained in the bivectors subspace (Table 3).

Another example that supports the claim that NNs need a large training set is found in [24]. Using 170 skin lesion images in ratio 25%/75% for testing/training, the authors received 77.1% accuracy of classification. While using 2000 images for training and 600 for testing from the ISBI2017 challenge dataset [7], they received an accuracy of 83.2%. The best accuracy ever achieved with the NN from [24] is 87.2% but the authors extended the training set by adding other publicly available skin lesion image datasets, bringing the training set to tens of thousands.

Paper [8] reports two statistics of diagnoses conducted by 61 dermatologists on 40 melanoma images. The dermatologists applied the 4 most commonly used rules for melanoma diagnosis in clinical practice: ABCD rule [4, 19], Menzies rule, 7-points checklist, and pattern analysis [8] (Table 6).

Note, that paper [17] used the same sample set as we did in the present study, but applied a ternary SVM, which classified the 112 skin LFVs to three classes: benign, dysplastic nevi and malignant. Considering benign and dysplastic nevi as negative and malignant as positive the ternary SVM achieved  $AC = 84%$  [17].

Table 6 shows that the highest 1st and 2nd diagnosing accuracies are obtained with the original 5D LFVs (1-vectors) and 11D  $Cl_{5,0}$  subspaces; the highest sensitivity comes with the Menzies rule [8]; the highest specificity comes with the ternary SVM 98%, while the 2nd highest specificity is obtained in the 11D Clifford subspace.

However we would like to note that the very high specificity obtained by the ternary SVM may come on the expense of using three binary SVMs that compose the ternary SVM and the use of  $\nu = 0.2$  [17]. On the other hand a single binary SVM is applied in the 11D Clifford subspace and  $\nu = 0.4$ .

	train/test	AC	SE	SP
1-vector $Cl_{5,0}$ subspace	110/2	84.7	82.4	86.4
bivector $Cl_{5,0}$ subspace	110/2	81.9	79.3	85.3
3-vector $Cl_{5,0}$ subspace	110/2	79	76.6	81.4
4-vector $Cl_{5,0}$ subspace	110/2	72.7	67.7	77.2
11D vectors $Cl_{5,0}$ subspace	110/2	84	79	87.2
[17] Ternary SVM	111/1	84	76	98
[8] ABCD rule	0/40	N/A	77	80
[8] Menzies rule	0/40	N/A	86	77.7
[8] Pattern analysis	0/40	N/A	60.9	85.5
[8] 7-point checklist	0/40	N/A	81	73
[9] CNN	129450/1942	72.1	N/A	N/A
[24] CNN	2000/600	83.2	N/A	N/A

Table 6. Classification in 1-, 2-, 3-, 4-vector 11D Clifford subspaces and the ternary SVM are conducted on the same set of 112 LFVs. Train means the number of samples used for training the SVM, while test shows the number of samples used for classification.

Note Menzies rule uses negative and positive skin LFs. The forward set consists of the symmetry of lesion structures and single color. The positive set includes brown dots; peripheral black dots/globules; blue gray dots; 5 or 6 colors; broadened networks; scare-like depigmentation; radial streaming and pseudopods. A lesion is diagnosed as melanoma if none of the negative and at least one of the positive features is present.

Equation (4.2) shows that a zero entry in an original LFV  $U_i$  generates several zero entries in the multivector  $A_{U_i}$ . Hence, the distances among the vectors in the corresponding  $Cl_{5,0}$  subspace decrease. It follows that the separability of the vectors decreases as well, leading to a lower accuracy of classification.

Note that a number of LFVs  $U_i$  have a 0 as an entry in the original 5D sample set of 112 LFVs. Equation (4.2) states that a 0 in an entry of  $U_i$  spreads to four 0s in the 4- and 2-vectors  $\langle A_U \rangle_4$  and  $\langle A_U \rangle_2$  respectively, while the 3-vector  $\langle A_U \rangle_3$  will have six 0s. Recall that the 4-vector is a 4D vector, while the 2-vector and 3-vector are 10D vectors. It follows that the 4-vector has the highest ratio between zero and non zero entries, which leads to the expectation that the 4-vector subspace will give the lowest classification rates. This conclusion is confirmed by the results reported in Tables 1 to 4.

Equation (3.5) implies that a 0 in the original 5D vector (1-vector) will not spread among the 11D vector entries. This fact and the vector larger dimension provide the highest rates of classification in the 11D  $Cl_{5,0}$  subspace as compared to the 2-, 3-, 4-subspaces (Tables 3–6).

The results presented in this paper reveal the high potential of using CAs and their subspaces in the analysis and classification of medical images. Hence, our future study continues with the development of Clifford SVM and Clifford NN.

## 7. APPENDIX

To estimate the accuracy, specificity and sensitivity of classification in the entire population we calculate the confidence intervals (CIs) applying the formulae [1]

$$(7.1) \quad AC - Z_{\alpha/2} \sqrt{\frac{AC(1-AC)}{n}} < \widehat{AC} < AC + Z_{\alpha/2} \sqrt{\frac{AC(1-AC)}{n}},$$

$$(7.2) \quad SP - Z_{\alpha/2} \sqrt{\frac{SP(1-SP)}{n}} < \widehat{SP} < SP + Z_{\alpha/2} \sqrt{\frac{SP(1-SP)}{n}},$$



$$(7.3) \quad SE - Z_{\alpha/2} \sqrt{\frac{SE(1-SE)}{n}} < \widehat{SE} < SE + Z_{\alpha/2} \sqrt{\frac{SE(1-SE)}{n}}.$$

In (7.1),  $AC$  denotes the accuracy of success in a set of  $n$  samples,  $\widehat{AC}$  the accuracy in the entire population, while  $Z_{\alpha/2}$  is a constant given by a statistical table [1]. We use in this paper  $\alpha = 0.05$ , construct CIs with confidence  $100(1 - 0.05)\%$ , and in this case  $Z_{\alpha/2} = 1.96$ . Further, we use  $n = 2000$ , because the results reported in Tables 3 and 4 are obtained from 1000 experiments and in each of them we hold out 2% (2) of the samples for testing.

In (7.2),  $SP$  denotes the specificity of binary classification in the sample set of  $n$  samples, while  $\widehat{SP}$  is the specificity of classification in the entire population. Same holds for  $SE$  and  $\widehat{SE}$  sensitivity in (7.3).

**Acknowledgement.** The authors thank to the anonymous reviewers for the useful recommendations and corrections which improved the quality of the paper. Also, our thanks go to the graduate student C. Parks for the initial SVM and to Dr. T. Boucher for the discussion on confidence intervals.

### References

- [1] *A. Agresti, B. A. Coull*: Approximate is better than “exact” for interval estimation of binomial proportions. *Am. Stat.* 52 (1998), 119–126.  
- [2] *American Cancer Society*: Cancer Facts & Figures. American Cancer Society, Atlanta, 2010; Available at <https://www.cancer.org/research/cancer-facts-statistics/all-cancer-facts-figures/cancer-facts-figures-2010.html>.
- [3] *J. L. Aragón, G. Aragon-Camarasa, G. Aragón-González, M. A. Rodríguez-Andrade*: Clifford algebra with mathematica. Available at <https://arxiv.org/abs/0810.2412> (2018), 10 pages.



- [4] *G. Argenziano, H. P. Soyer, V. De Giorgi, D. Piccolo*: Dermoscopy: A Tutorial. Edra Medical Publishing & New Media, Milan, 2000.
- [5] *C. Barata, M. E. Celebi, J. S. Marques*: A survey of feature extraction in dermoscopy image analysis of skin cancer. *IEEE J. Biomedical and Health Inf.* *23* (2018), 1096–1109. doi
- [6] *E. J. Bayro-Corrochano, N. Arana-Daniel*: Clifford support vector machines for classification, regression, and recurrence. *IEEE Trans. Neural Networks* *21* (2010), 1731–1746. doi
- [7] *N. C. F. Codella, D. Gutman, M. E. Celebi, B. Helba, M. A. Marchetti, S. W. Dusza, A. Kalloo, K. Liopyris, N. Mishra, H. Kittler, A. Halpern*: Skin lesion analysis toward melanoma detection: A Challenge at the 2017 International Symposium on Biomedical Imaging (ISBI), Hosted by the International Skin Imaging Collaboration (ISIC). Available at <https://arxiv.org/abs/1710.05006> (2017), 5 pages.
- [8] *C. Dolianitis, J. Kelly, R. Wolfe, P. Simpson*: Comparative performance of 4 dermoscopic algorithms by nonexperts for the diagnosis of melanocytic lesions. *Arch. of Dermatology* *141* (2005), 1008–1014. doi
- [9] *A. Esteva, B. Kuprel, R. A. Novoa, J. Ko, S. M. Swetter, H. M. Blau, S. Thrun*: Dermatologist-level classification of skin cancer with deep neural networks. *Nature* *542* (2017), 115–118. doi
- [10] *G. P. Guy, D. U. Ekwueme, F. K. Tangka, L. C. Richardson*: Melanoma treatment costs: A systematic review of the literature, 1990–2011. *Am. J. Prev. Med.* *43* (2012), 537–545. doi
- [11] *B. Harangi*: Skin lesion classification with ensembles of deep convolutional neural networks. *J. Biomedical Inf.* *86* (2018), 25–32. doi
- [12] *M. H. Jafari, S. Samavi, N. Karimi, S. M. R. Soroushmehr, K. Ward, K. Najarian*: Automatic detection of melanoma using broad extraction of features from digital images. Engineering in Medicine and Biology Society (EMBC), Annual International Conference of the IEEE. IEEE, New York, 2016, pp. 1357–1360. doi
- [13] *K. Korotkov*: Automatic Change Detection in Multiple Skin Lesions. Ph.D. Thesis, Universitat de Girona, Girona, 2014.
- [14] *P. Lounesto*: Clifford Algebras and Spinors. London Mathematical Society Lecture Note Series 286, Cambridge University Press, Cambridge, 2001. zbl MR doi
- [15] *A. Masood, A. A. Al-Jumaily*: Computer aided diagnostic support system for skin cancer: a review of techniques and algorithms. *Int. J. Biomedical Imaging* *2013* (2013), Article ID 323268, 22 pages. doi
- [16] *M. Mete, N. M. Sirakov*: Dermoscopic diagnosis of melanoma in a 4D feature space constructed by active contour extracted features. *Computerized Medical Imaging and Graphics* *36* (2012), 572–579. doi
- [17] *M. Mete, N. M. Sirakov, J. Griffin, A. Menter*: A novel classification system for dysplastic nevus and malignant melanoma. IEEE International Conference on Image Processing (ICIP). IEEE, New York, 2016, pp. 3414–3418. doi
- [18] *B. Mishra, P. R. Wilson, R. Wilcock*: A geometric algebra co-processor for color edge detection. *Electronics* *4* (2015), 94–117. doi
- [19] *F. Nachbar, W. Stolz, T. Merkle, A. B. Cognetta, T. Vogt, M. Landthaler, P. Bilek, O. Braun Falco, G. Plewig*: The ABCD rule of dermatoscopy. High prospective value in the diagnosis of doubtful melanocytic skin lesions. *J. Am. Acad. Dermatol.* *30* (1994), 551–559. doi
- [20] *S. Roy, A. Mitra, S. K. Setua*: Color image representation using multivector. 5th International Conference on Intelligent Systems, Modelling and Simulation. IEEE, Langkawi, 2014, pp. 27–29. doi
- [21] *R. Schott, G. S. Staples*: Reductions in computational complexity using Clifford algebras. *Adv. Appl. Clifford Algebr.* *20* (2010), 121–140. zbl MR doi

- [22] *N. Singh, S. K. Gupta*: Recent advancement in the early detection of melanoma using computerized tools: An image analysis perspective. *Skin Res. Technol.* *25* (2019), 129–141. [doi](#)
- [23] *N. M. Sirakov, M. Mete, R. Selvaggi, M. Luong*: New accurate automated melanoma diagnosing systems. *International Conference on Healthcare Informatics. IEEE, Dallas, 2015*, pp. 374–379. [doi](#)
- [24] *N. N. Sultana, B. Mandal, N. B. Puhan*: Deep residual network with regularized fisher framework for detection of melanoma. *IET Computer Vision* *12* (2018), 1096–1104. [doi](#)
- [25] *J. Vaz, Jr., R. da Rocha, Jr.*: *An Introduction to Clifford Algebras and Spinors*. Oxford University Press, Oxford, 2016. [zbl](#) [MR](#) [doi](#)
- [26] *M. A. Wahba, A. S. Ashour, Y. Guo, S. A. Napoleon, M. M. Abd Elnaby*: A novel cumulative level difference mean based GLDM and Modified ABCD features ranked using eigenvector centrality approach for four skin lesion types classification. *Computer Methods and Programs in Biomedicine* *165* (2018), 163–174. [doi](#)
- [27] *Z. Yu, X. Jiang, F. Zhou, J. Qin, D. Ni, S. Chen, B. Lei, T. Wang*: Melanoma recognition in dermoscopy images via aggregated deep convolutional features. *IEEE Trans. Biomed. Eng.* *66* (2019), 1006–1016. [doi](#)

*Authors' addresses: Mutlu Akar, Yildiz Technical University, College of Arts and Sciences, Department of Mathematics, 34210, Istanbul, Turkey, e-mail: [makar@yildiz.edu.tr](mailto:makar@yildiz.edu.tr); Nikolay Metodiev Sirakov, Texas A&M University-Commerce, Department of Mathematics, P.O. Box 3011, 75429, Commerce, TX, USA, e-mail: [Nikolay.Sirakov@tamuc.edu](mailto:Nikolay.Sirakov@tamuc.edu).*